Astron. Astrophys. 157, 318–328 (1986)

ASTRONOMY AND ASTROPHYSICS

The centimeter transitions of *E*-type methanol

K.M. Menten, C.M. Walmsley, C. Henkel, and T.L. Wilson

Max-Planck-Institut für Radioastronomie, D-5300 Bonn 1, Auf dem Hügel 69, Federal Republic of Germany

Received July 15, accepted August 30, 1985

Summary. We have used the 100-m telescope at a frequency of 25 GHz to observe the $2_2 \rightarrow 2_1$, $3_2 \rightarrow 3_1$, $4_2 \rightarrow 4_1$, $5_2 \rightarrow 5_1$, $6_2 \rightarrow 6_1$, and $9_2 \rightarrow 9_1$ transitions of *E*-type methanol towards a selection of galactic molecular-line sources. We have found several sources of strong narrow line emission in these transitions which we believe to be masers similar to those known in the Orion-KL region. Their power output, line widths, and *J*-dependence are similar to the Orion values. They often appear well separated from compact H II regions, strong infrared sources and other indicators of the formation of high mass stars. We also observe absorption in these lines towards W3(OH) and NGC 7538 showing that the transitions are not necessarily inverted under interstellar conditions. Finally, most strong molecular line sources show emission in these transitions with a profile similar to that known from observations of other molecules. The rotation temperatures estimated for such emission features range between 20 and 100 K. We conclude that we are observing hot (100 K) compact (10^{17} cm) clumps immersed in the general molecular cloud material, which is preferentially sampled, for example, in surveys of the $J = 2 \rightarrow 1$ methanol transitions.

Key words: molecular cloud – methanol – masers

1. Introduction

Maser emission in the $J_{k=2} \rightarrow J_{k=1}$ ($J = 2, 3, 4, 5, 6, 7$) series of transitions of interstellar methanol (CH_3OH) has been known for some time (Barrett et al., 1971). However, Orion K-L has remained the only source to show this type of behavior (Buxton et al., 1977) despite the fact that methanol is clearly a widespread molecule (Gottlieb et al., 1979; Boland et al., 1983). Moreover, the millimeter ($\Delta J = 1$) transitions observed up to now have been well behaved in the sense that the derived population ratios are thermal or sub-thermal. Hence the K-band masing transitions are something of an anomaly and their astrophysical interpretation is still obscure. The situation has recently been further complicated by the discovery that the $9_2 \rightarrow 10_1 A^+$ and $2_1 \rightarrow 3_0 E$ transitions (Wilson et al. (1984), Menten et al. (1985), Wilson et al. (1985)) are strongly masing towards the compact H II region W3(OH). These lines are sometimes seen in absorption however towards other sources. Also, Morimoto et al. (1984) find maser emission in the $4_{-1} \rightarrow 3_0 E$ and $7_0 \rightarrow 6_1 A$ lines observed towards Sgr B2 and three other galactic sources. All of these phenomena have different spatial distributions and line width characteristics and presumably sample different regions. In this situation, it seemed worthwhile to examine with high sensitivity a large sample of sources in the $J_2 \rightarrow J_1$ series of *E* type CH_3OH (see Fig. 1) in order to check both for masers outside Orion as well as for quasithermal emission where present.

Send offprint requests to: C.M. Walmsley

2. Observations

Observations of the $2_2 - 2_1$, $3_2 - 3_1$, $4_2 - 4_1$, $5_2 - 5_1$, $6_2 - 6_1$, and $9_2 - 9_1$ transitions of *E*-type CH_3OH at frequencies varying between 24.9 and 25.5 GHz have been carried out with the 100-m telescope equipped with a K-band maser. System temperatures were typically of the order of 80 K. The beamwidth at these frequencies is approximately 38 arcsec. Details of the sources, measured transitions and observing dates are given in Table 1.

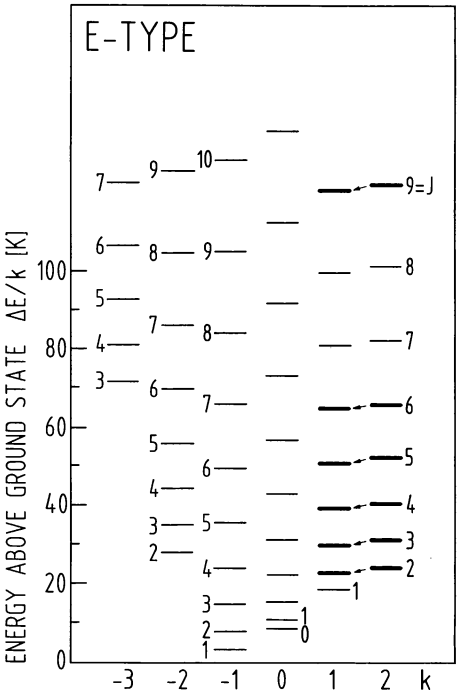

Fig. 1. Level diagram for the lower transitions of *E*-type methanol. The thick lines denote the levels connected by the $J_2 \rightarrow J_1$ series of lines which have been observed by us

Table 1. Summary of measurements of sources searched in the $J_2 \rightarrow J_1$ series of CH_3OH

Source	α (1950)	δ (1950)	v_{cen} km s^{-1}	Em/Abs.	Transitions observed: J = 2, 3, 4 Date 4/84	J = 2, 3, 4 3/85	J = 5, 6 9/84	J = 5, 6 3/85	J = 6 2/84	J = 6 9/84	J = 9 9/84
W3(OH)	02 23 17.0	61 38 53	-45	E/A	x[a]	-	x[a]	-	-	-	-
Ori-A KL	05 32 46.7	-05 24 21	9	M,E	-	-	-	-	x	-	-
Ori-S6	05 32 45.3	-05 26 02	9	E,M?	-	-	-	-	x[b]	-	-
Mon R2	06 05 19.5	-06 22 48	8	-	-	-	-	-	x	-	-
R Leo	09 44 52.2	11 39 41	-1	-	x	-	-	-	-	-	-
IRC10216	09 45 14.8	13 30 40	-25	-	x	-	-	-	-	-	-
W Hya	13 46 12.1	-28 07 02	40	-	x	-	-	-	-	-	-
U Her	16 23 34.8	19 00 17	-15	-	x	-	-	-	-	-	-
Sgr A	17 42 27.9	-29 04 00	15	E	x	-	-	-	-	-	-
Sgr B2	17 44 10.6	-28 22 00	60	E	x[c]	x	x[d]	-	-	-	-
W31	18 07 30.6	-19 56 30	0	E,M	x	-	-	x[b]	x	x[e]	x
W33B	18 10 59.4	-18 02 47	40	-	x	-	-	-	-	-	-
W33	18 11 18.5	-17 56 46	40	E,M	x[f]	-	x[g]	-	-	-	-
W33A	18 11 44.5	-17 52 56	40	E	x	-	-	-	-	-	-
OH26.5+0.6	18 34 52.5	-05 26 40	27	-	x	-	-	-	-	-	-
W51D	19 21 22.1	14 25 15	60	E,M	x[e]	x[h]	-	x[i]	-	-	x[h]
W51E	19 21 24.7	14 24 52	60	E,M	x	x[h]	-	x[i]	-	x[j]	x[h]
χ Cyg	19 48 38.5	32 47 11	9	-	x	-	-	-	-	-	-
K3-50	19 59 50.1	33 24 17	-20	-	x	-	-	-	-	-	-
ON1	20 08 10.0	31 22 40	11	E	x	-	-	-	-	-	-
ON2	20 19 52.0	37 17 01	-5	-	x	-	-	-	-	-	-
CRL2591	20 27 36.0	40 01 16	-1	E	-	-	-	-	-	x	-
W75N	20 36 50.0	42 26 57	-2	E	x	-	-	-	-	-	-
DR21(OH)	20 37 13.8	42 12 00	0	E	x	-	x[a]	x	-	x	x
DR21	20 37 14.2	42 09 06	-3	E,M	x	x[e,k]	-	x[e]	x	-	x
NML Cyg	20 44 33.8	39 56 00	0	-	x	-	-	-	x	-	-
V645 Cyg	21 38 11.0	50 00 23	-45	-	-	-	-	-	-	x	-
S140	22 17 41.2	63 03 41	-6	E	x	-	-	-	-	-	-
Ceph A	22 54 19.0	61 45 47	-8	-	x	-	-	-	-	-	-
NGC7538	23 11 36.7	61 11 53	-55	A	x	-	x[l]	-	-	-	x

Notes: If not otherwise noted, all offsets are in (α,δ) relative to the given reference position
a) 9 pt map with 40" offsets
b) Measurements at ±20" offsets
c) Offsets of (-40,0), (0,-40), (0,0), (0,40), (0,80), (0,120), (40,0)
d) For offsets in α of -40", 0", and 40", strips in δ ranging from -80" to 120" were made
e) Measurements at ±40" offsets
f) Offsets of (-80,0), (-40,-40), (-40,0), (-40,40), (0,-40), (0,0), (0,40), (40,0)
g) Measurements include 9 pt map centred on α(1950) = $18^h11^m16^s.0$, δ(1950) = -17°56'45"
h) Measurements at approximate maser positions (see text)
i) Measurements at ±20" offsets from approximate maser positions
j) Offsets of (-80,-120), (-80,-80), (-80,-40), (-80,0), (-80,40), (-80,40), (-80,80), (-40,-40), (-40,0), (-40,40), (-40,80), (0,-40), (0,0), (0,40), (0,80), (0,120), (40,-120), (40,-80), (40,-40), (40,0), (40,40) (80,-40), (80,0), (80,40)
k) Offsets of (-80,-20), (-60,-20), (-40,-40), (-40,-20), (-40,0), (-20,-20)
l) 9 pt map with 40" offsets centred on (0,-40)

The positions given here are used as reference positions elsewhere in this article. For the $J = 2, 3, 4$ observations in April 1984, a 384 channel autocorrelator was split into two receivers in order to simultaneously measure the $J = 2$ and 4 lines in one and the $J = 3$ line in the other. Using a bandwidth of 10 MHz per receiver, the velocity resolution was $\sim 0.6\,km\,s^{-1}$. On all other observing dates, a 1024 channel autocorrelator was available yielding for the standard bandwidth of 12.5 MHz velocity resolutions of $0.15\,km\,s^{-1}$ per channel in unsplit and $0.3\,km\,s^{-1}$ in split mode. In several cases, spectra were taken at higher resolutions.

The flux density scale has been established assuming a flux for NGC 7027 of 5.8 Jy. Uncertainties in our derived fluxes due to pointing errors or fluctuations in atmospheric attenuation are of order twenty percent. To convert our flux scale to one of main-beam brightness temperature, one should multiply by 1.4. In cases where continuum sources were present, we made a continuum scan prior to the line observations. This allows us to express the absorption line intensity more physically in terms of the line-to-continuum ratio. Parameters for the detected absorption lines are given in Table 2 and for emission lines in Table 3.

3. General results

We detected the $J_2 \rightarrow J_1$ transitions toward most well known molecular cloud positions but not towards late type stars (see

Table 2. Absorption line parameters

		W3(OH)[a]	NGC7538
T_L/T_C	J=2	0.056(0.011) -0.14 (0.02) -0.14 (0.02)	-0.10(0.01)
	3	0.10 (0.03) -0.17 (0.05) -0.11 (0.13)	-0.10(0.01)
	4	0.075(0.012) -0.17 (0.04) -0.11 (0.03)	-0.10(0.01)
	5	0.065(0.006) -0.18 (0.01) -0.11 (0.01)	-0.09(0.01)
	6	0.050(0.003) -0.20 (0.01) -0.12 (0.01)	-0.11(0.01)
	9	0.035(0.007) -0.17 (0.01) -0.11 (0.01)	-0.13(0.01)
V_{LSR}(J=6) [km s^{-1}]		-47.1(0.3) -45.0(0.2) -43.7(0.4)	-59.9(0.1)
Δv(J=6) [km s^{-1}]		6.6(0.6) 1.0(0.1) 1.1(0.1)	4.6(0.3)
T_R [K]		73(7)[b]	85(14)
$N(CH_3OH)$ [cm^{-2}]		7.9 10^{14} T_{ex} [b]	1.3 10^{15} T_{ex}

Notes: a) One emission (at v=-47.1 km s^{-1}) and two absorption (at -45.0 and -43.7 km s^{-1}) gaussian components were fitted to the W3(OH) spectra
b) This value was determined using the absorption components

Table 1). Figures 2 and 3 show spectra obtained towards W3(OH), W31, W33, DR21 (OH) and NGC 7538 in a series of $J_2 - J_1$ E-type transitions. Towards W31 and W33 one sees in the $4_2 \rightarrow 4_1$ and higher J lines evidence for narrow band emission with $\Delta v \sim 0.3$–$0.5\,\mathrm{km\,s^{-1}}$. Such narrow lines are typical of interstellar masers (see Reid and Moran, 1981) and we shall describe them as maser lines in the following discussion. They are spatially unresolved with our beam and appear to have characteristics similar to the well known Orion methanol masers (see below and Matsakis et al., 1980). They are often superimposed upon wider emission features which are most prominent in the $J = 2$–4 lines. These broader emission lines have parameters compatible with formation in the general molecular cloud gas. Towards W3(OH) and NGC 7538, we see absorption in all observed transitions (Fig. 2). This is important because it shows that the $J_2 \rightarrow J_1$ lines are not always inverted in molecular clouds. We can derive the apparent optical depth or line to continuum ratio for such transitions by comparing our line measurements with the results of narrow band continuum scans. This gives a limit to the true optical depth in these lines.

In view of this behavior, it is useful to discuss the narrow band "maser" sources, the broad emission features and the absorption separately although they are not necessarily independent phenomena. We start by a brief résumé of the properties of the maser features.

3.1. Maser features

Table 4 gives positions where we have observed narrow band features and summarises their properties. As far as we can judge, there is no clear correlation between methanol maser positions and either radio continuum or far infrared emission. The maser in W33, for example, is 45″ west of the compact continuum source and the two masers in W31 are ~10″ north-east of the source W31C (G10.6, Ho and Haschick (1981)). The masers in W51 (see Fig. 4) are in the general area of the molecular cloud emission but are not coincident with infrared or radio sources.

The behavior of observed maser fluxes as a function of J is very similar to that observed in Orion. This is shown in Fig. 5 where we compare results for several sources with observations of Orion by Matsakis et al. (1980). In general, for our sources, there is a maximum in the range $J = 5$–7 with a very sharp rise between $J = 2$ and 5. One exception is the $v = 54\,\mathrm{km\,s^{-1}}$ maser in W51 where the $J = 6$ and 9 lines have approximately equal intensity (see Fig. 5). Table 4 also gives the integrated photon luminosity in the $6_2 \rightarrow 6_1$ transition due to the narrow band features. These values are similar to those in Orion (1–$2\,10^{43}$ photons s^{-1}). We note also that offset measurements of the narrow band features are consistent with source sizes less than 30″. Hence, we believe that they are "Orion-type" masers and that the Orion masers are not unique. It is relevant in this context that the Orion masers themselves do not show obvious correlation with infrared peaks in the Kleinmann-Low nebula (Matsakis et al., 1980).

A point of importance here is that the Orion masers have been shown to be variable on a time scale of months (Barrett et al., 1975). One would therefore expect similar variability in the new maser sources. This is not presently evident in our data. We note too that the relative intensity of the $v = -6$ and $-8\,\mathrm{km\,s^{-1}}$ masers in W31 (which are separated by ~1–2 arcsec) has not changed between February 1984 and March 1985 by more than ten percent. It also seems to be a property of the Orion maser components that their relative intensity does not change greatly and this may be a clue to the excitation mechanism.

3.2. Absorption lines in NGC 7538 and W3(OH)

We observe pure absorption in all transitions towards NGC 7538 and a mixture of emission and absorption towards W3(OH) (Fig. 2). The excitation temperatures of the transitions where absorption is seen are certainly positive and less than the brightness temperature of the background continuum radiation, which is 1000 K for NGC 7538 and 3000 K for W3(OH). Table 2 summarises the derived line parameters for the two sources. We note that a fit to the observed profiles in W3(OH) is a highly subjective process. Of particular interest is the "double" nature of the absorption apparent in the transitions higher than $5_2 \rightarrow 5_1$. It is conceivable that this is an artifact caused by a weak maser at a velocity of $-44\,\mathrm{km\,s^{-1}}$ which partially fills the absorption trough. If such a maser had a J-dependence similar to the sources in Fig. 5, it would not be visible in the lower transitions ($2_2 \rightarrow 2_1$, $3_2 \rightarrow 3_1, 4_2 \rightarrow 4_1$) but might be time variable. Our measurements in February and September 1984 suggest that over this time interval the "emission" feature has not varied more than 30%. Measurements at positions 40″ offset from the continuum peak in the $5_2 \rightarrow 5_1$ and $6_2 \rightarrow 6_1$ transitions show no feature stronger than 0.5 Jy. Hence, we consider it likely that there are two or more velocity components giving rise to the absorption towards

Table 3. Thermal emission line parameters

Source[a]	$\int T_L dv$ [K km s^{-1}] J = 2	3	4	5	6	9	v_{LSR}[b] [km s^{-1}]	Δv[b] [km s^{-1}]	Notes
Orion S-6	-	-	-	-	5.3(0.3)	-	7.0(0.1)	3.9(0.2)	c)
Sgr A	∿5	∿4	∿5	-	-	-	∿14	∿12	
Sgr B2(-40,0)	50.0(4.6)	56.6(2.5)	46.8(4.4)	29.8(2.2)	24.3(1.7)	-	61.8(0.3)	24.4(0.9)	
" " (0,-40)	40.3(3.0)	44.5(1.6)	32.3(2.7)	17.0(2.8)	8.9(1.2)	-	61.9(0.2)	17.2(0.5)	
" " (0,0)	23.8(3.7)	51.8(1.5)	71.4(4.7)	27.7(1.3)	21.3(1.0)	-	63.0(0.1)	16.2(0.4)	
" " (0,40)	44.8(11.4)	54.9(2.1)	56.5(9.1)	39.3(2.7)	28.3(1.8)	-	64.9(0.2)	15.0(0.5)	
" " (0,80)	37.9(6.4)	39.3(3.3)	15.4(4.6)	24.1(2.5)	14.6(2.3)	-	69.8(0.5)	24.3(1.6)	
" "(0,120)	24.0(6.2)	17.6(2.5)	8.6(3.5)	<13	<11	-	65.9(0.9)	25.4(2.9)	
" "(40,0)	23.6(3.3)	20.1(1.5)	7.6(2.0)	7.3(1.8)	<8.5	-	60.9(0.4)	21.5(1.3)	
W31C	2.0(0.4)	4.7(0.5)	3.6(0.6)	5.1(0.8)	4.0(0.6)	<2.5	-2.6(0.2)	6.5(0.6)	
W33(-40,-40)	<0.7	0.8(0.4)	<0.7	-	-	-	35.2(0.5)	3.9(1.2)	
" (-40,0)	1.2(0.4)	1.7(0.2)	1.6(0.4)	-	-	-	36.7(0.2)	3.9(0.5)	
" (-40,40)	1.2(0.2)	-	1.2(0.2)	-	-	-	35.0(0.3)	3.3(0.6)	d)
" (0,0)	6.6(0.5)	10.2(0.5)	8.6(0.5)	9.8(1.2)	8.8(0.9)	-	36.3(0.1)	5.7(0.2)	
" (0,40)	3.5(0.7)	3.4(0.6)	2.2(0.5)	-	-	-	35.3(0.2)	3.4(0.5)	
" (40,0)	<1.2	1.3(0.7)	<1.2	-	-	-	36.1(0.6)	3.7(1.4)	
W33A	1.8(0.3)	-	1.0(0.3)	-	-	-	36.7(0.3)	5.5(1.3)	d)
W51D	5.2(1.1)	3.9(0.5)	4.3(0.7)	-	3.6(0.3)	2.9(0.2)	59.5(0.4)	8.8(0.9)	
W51E(0,0)	3.3(0.4)	4.5(0.3)	5.2(0.6)	7.7(0.6)	6.4(0.6)	<1.7	57.7(0.3)	10.5(0.6)	
" (0,40)	1.8(0.3)	1.9(0.3)	1.8(0.3)	1.6(0.3)	1.0(0.3)	<1.5	61.0(0.4)	8.1(0.9)	
" (40,-40)	2.7(0.4)	2.8(0.3)	2.8(0.4)	3.4(0.3)	3.0(0.3)	2.2(0.5)	55.4(0.2)	7.4(0.6)	
ON1	0.62(0.21)	0.56(0.25)	0.50(0.22)	-	-	-	11.9(0.3)	3.3(0.6)	
CRL 2591	-	-	-	-	0.36(0.13)	-	-5.6(0.3)	2.1(0.6)	c)
W75N	0.87(0.18)	0.96(0.23)	1.18(0.21)	-	-	-	9.4(0.3)	3.8(0.6)	
DR21(OH)	3.0(0.6)	4.3(0.5)	4.7(0.5)	3.4(0.4)	3.2(0.4)	0.6(0.1)	-2.9(0.2)	5.7(0.5)	
DR21	2.0(0.5)	3.0(0.2)	2.6(0.7)	2.0(0.2)	1.9(0.2)	-	-2.0(0.1)	3.9(0.2)	
S140	0.47(0.14)	0.40(0.12)	0.32(0.15)	-	-	-	-6.9(0.2)	2.8(0.7)	

Notes: a) Offsets are relative to the positions given in Table 1
b) If not otherwise noted, v_{LSR} and Δv of 3_2-3_1 E line are given
c) v_{LSR} and Δv of 6_2-6_1 E line are given
d) v_{LSR} and Δv of 4_2-4_1 E line are given

W3(OH). We have derived the ratio of column density in the lower level $N(J_1)$ to excitation temperature T_{ex} using the formula:

$$N(J_1)/T_{ex}\,(\mathrm{cm}^{-2}/\mathrm{K}) = 8.57\,10^{13}(2J+1)\tau(J_2 \rightarrow J_1)\,\Delta v\,(\mathrm{km\,s}^{-1})/(S(J_2 \rightarrow J_1)\nu(\mathrm{GHz})) \quad (1)$$

where S is line strength (Lees et al., 1973; Lees, 1973) and ν is the line frequency in GHz. Here, we assumed optically thin conditions and $T_{ex} \gg h\nu/k \approx 1$ K. In Fig. 6, we plot the derived $N(J_1)/T_{ex}$ for W3(OH) and NGC 7538 against the excitation energy of the J_1 level $E_{ex}(J_1)$. From this plot, we derive an "apparent" rotation temperature (i.e. assuming T_{ex} not to vary with J) of 73 K for W3(OH) and 85 K for NGC 7538. The assumption of constant T_{ex} is almost certainly not valid however, and moreover the lines may be optically thick. We note that for both W3(OH) and NGC 7538 (see Table 3), the line-to-continuum ratio is of order 0.1–0.15. The actual optical depth depends upon the fraction of the continuum source covered by the methanol cloud. This is unknown but experience with A-type methanol (Menten et al., 1985) suggests that methanol is abundant in the absorbing cloud where ammonia and OH-masers are found. The ammonia absorption has a covering factor of 0.3 in W3(OH) and 0.17 in NGC 7538 (Pauls and Wilson, 1980; Henkel et al., 1984). We suspect therefore that the optical depth in the methanol lines examined by us is at least 0.3 towards W3(OH) and 0.9 towards NGC 7538. In view of these uncertainties, the rotation temperatures, which we derive, give only a rough guide to the molecular excitation.

The absorption seen in W3(OH) may be related to the emission seen at velocities more negative than $-46\,\mathrm{km\,s}^{-1}$. Such features are also seen in ammonia, and the similarity between the behavior of ammonia and methanol is very striking. Guilloteau et al. (1983) have suggested that the ammonia is mainly present in a torus like structure surrounding the compact H II region and the same may be true for methanol. The foreground portion of the torus is seen in absorption and the rest in emission. The similarity with the ammonia profiles makes it unlikely that we are observing a superposition of maser features but the possibility cannot completely be excluded. We note also that, towards NGC 7538, while pure absorption is observed towards the compact continuum source (Fig. 2), we have detected an emission feature in the $6_2 \rightarrow 6_1$ line approximately 45″ to the south-west of NGC 7538-IRS1.

3.3. *Molecular cloud emission features*

In several sources, we observe emission with line widths in the range 1–10 km s^{-1}. In most cases, the line profiles are in reason-

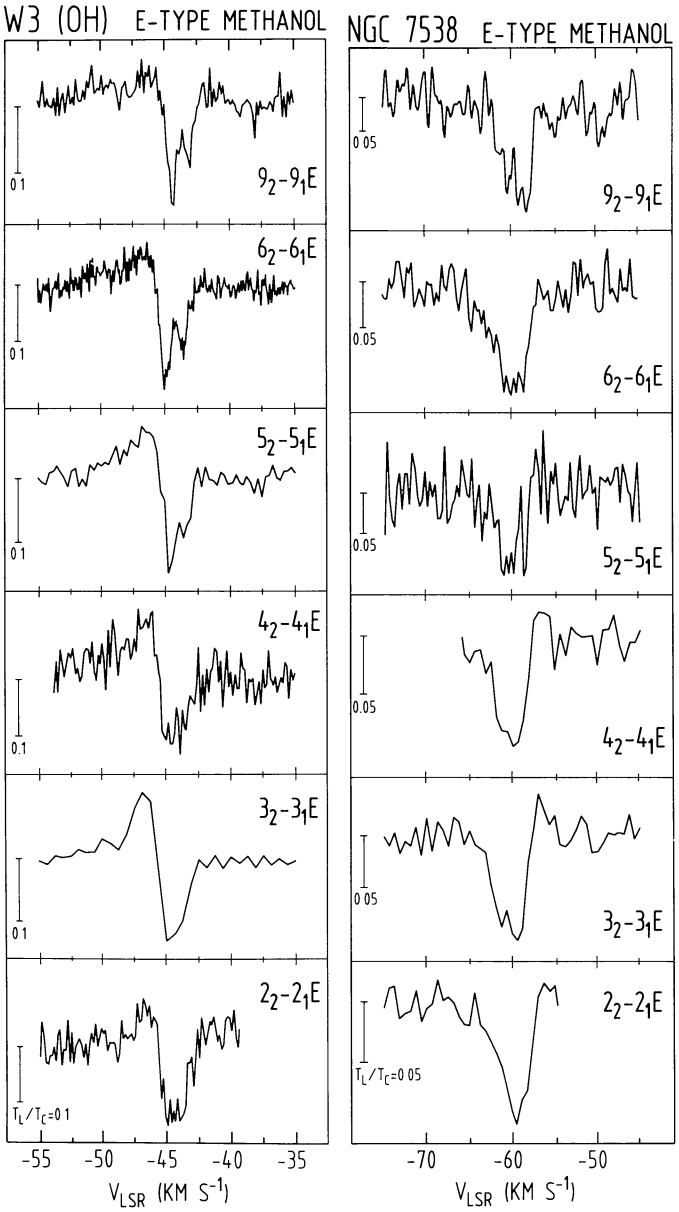

Fig. 2. Observed spectra towards W3(OH) and NGC 7538. The W3(OH) spectra show absorption to the red of $-47\,\mathrm{km\,s^{-1}}$ and emission to the blue.

able agreement with those found from observations of other molecules. For example, in DR21(OH) and W51, the measured velocity and line-widths are reasonably consistent with those found in the 96 GHz $J = 2 \rightarrow 1$ CH_3OH lines by Gottlieb et al. (1979). We therefore call these molecular cloud features and derive rotation temperatures assuming optically thin conditions (i.e. using Eq. (1) applied to the case of an emission line). On this basis, we plot in Fig. 7 $N(J_1)$ as a function of $E_{ex}(J_1)$ for a sample of sources. Table 5 summarises the derived rotation temperatures and column densities. We used the equation:

$$N(\mathrm{CH_3OH}) = 2Z\exp(E_J/kT_R)N(J_1)/g(J_1)$$

where the partition function $Z = 0.64T_R^{1.5}$, E_J is the excitation of the J_1 level in K and $g(J_1)$ is the statistical weight.

We now comment on several individual sources.

3.3.1. W31

In transitions up to and including $6_2 \rightarrow 6_1$, we see the maser features discussed earlier superimposed upon broad emission. This is in contrast to the $9_2 \rightarrow 10_1A^+$ and $2_1 \rightarrow 3_0E$ lines which are in absorption and $2\,\mathrm{km\,s^{-1}}$ to the red of the emission lines observed by us. Our offset measurements suggest that the broad emission feature is point-like and offset 5″ N of the compact continuum source W31C (or 6″ W and 3″ S of the maser positions). To obtain these positions, we checked the pointing on the continuum peak and made a 5-point map in the lines. Gaussian fits to the profiles were used to determine the offset position of the broad emission and maser features. From this procedure, our relative positions should be accurate to 1″.

3.3.2. W33

Limited offset measurements show that the broad feature seen towards the W33 continuum source is extended.

3.3.3. Sgr B2

Our measurements (see Table 5) show that the rotation temperature in Sgr B2 is low (~20 K). The line velocities and widths are comparable to those found for other molecules. Wilson et al. (1985) found the $2_1 \rightarrow 3_0E$ line to be in absorption towards this source with roughly similar parameters to the emission lines found by us. The $J_2 \rightarrow J_1$ series of lines may thus be inverted in Sgr B2 but have low optical depth. Our $6_2 \rightarrow 6_1$ observations show no narrow band masers towards this source although there is apparent maser activity in the $4_{-1} \rightarrow 3_0E$ line (Morimoto et al., 1984).

3.3.4. W51

Towards W51, we observe a feature with $v \sim 60\,\mathrm{km\,s^{-1}}$ and $\Delta v \sim 10\,\mathrm{km\,s^{-1}}$ (see Fig. 4). This profile is similar to that observed in ammonia (Mauersberger et al., 1985) and it is reasonable to suppose that the methanol lines are formed in the same volume as NH_3. The spatial distributions of the two molecules are also similar. The ammonia data suggest very high kinetic temperatures ranging up to 200 K towards W 51 D.

3.3.5. *DR21 (OH)*

The line parameters towards this source are compatible with those observed in ammonia (Mauersberger et al., 1985) and formaldehyde (Johnston et al., 1984). The 2 cm formaldehyde emission is thought to come from a region 0.15 pc in size with density $10^6\,\mathrm{cm^{-3}}$ and mass between 6 and 150 $M_\odot$. The methanol rotation temperature of 29 K compares with a kinetic temperature of 58 K derived from the NH_3 data.

4. Discussion

4.1. Maser source properties

For reasons discussed earlier, the narrow-line sources discovered in this work resemble well known Orion methanol masers. Hence, much of the discussion of the nature of the Orion masers is applicable to the sources in Table 4 (see Matsakis et al., 1980; Strel'nitskii, 1981). Our data are important in that they show that the near proximity of a massive young star is not a necessary condition for the existence of an E-type methanol maser. The

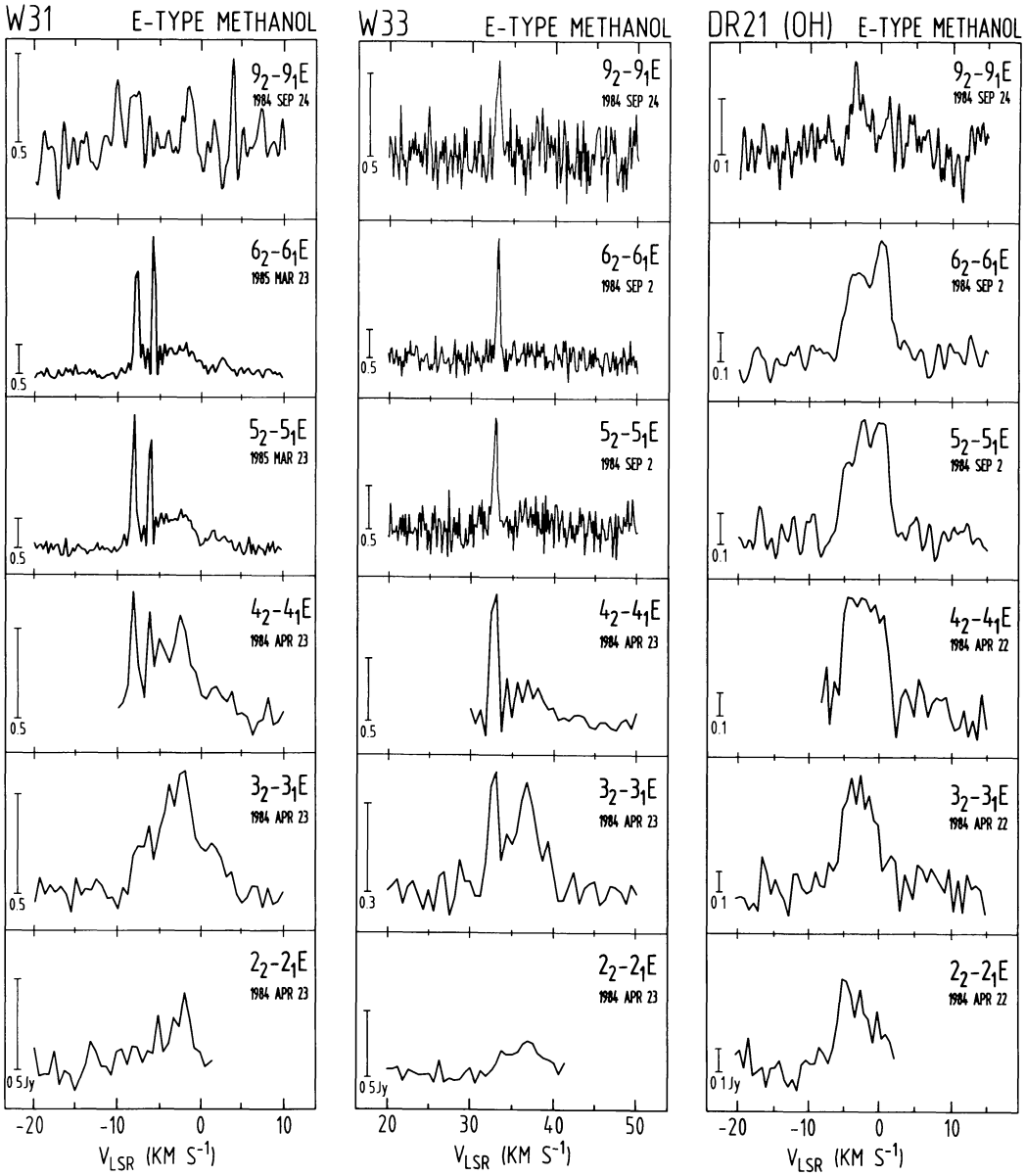

Fig. 3. Observed spectra towards W31, W33 and DR21 (OH). The W33 spectra were taken ~40″ west of the "continuum" position given in Table 1

maser which we have found in DR21 for example (see Table 4), is roughly 1 parsec in projected distance from the DR21 radio continuum source. It seems improbable that the ionizing stars of the H II region are powering the methanol maser. A search for low luminosity infrared objects in the vicinity of such masers might be profitable.

Assuming isotropic maser emission, we can derive rough lower limits for the luminosity of a hypothesised infrared radiative pump source. One expects at least one pump photon for every maser photon and hence to explain a maser output L_M (photons s^{-1}), one requires an infrared source of luminosity:

$$L_{IR} \approx L_M(h\nu_{IR}) \frac{c}{\Delta v} \text{ erg s}^{-1}.$$

ν_{IR} here is the frequency of the pump line and Δv is its linewidth. The factor $c/\Delta v$ corrects roughly for the fact that the pumping source radiates over a large bandwidth but is only effective within one of the methanol vibrational bands (see Table 7 of Matsakis et al., 1980). For $L_M = 2\,10^{43}$ photons s^{-1}, $\nu_{IR} = 6\,10^{12}$ Hz, and $\Delta v = 1$ km s^{-1}, we have then a lower limit for L_{IR} of 50 $L_\odot$. This should be observable in the 10–50 μm range and hence radiative pump mechanisms can be tested for. The nature of the CH_3OH masers may be much easier to determine in the newly discovered sources than in Orion due to the lesser confusion.

4.2. *Non-maser regions*

When one puts to one side the observations of OMC-1, methanol surveys to date have sampled relatively cool gas. For example, Boland et al. (1983) derived an excitation temperature of 90 K for Orion but upper limits of 25 K towards several other sources based upon their $J = 5 \rightarrow 4$ observations. Gottlieb et al. (1979)

Table 4. Positions and $6_2 - 6_1 E$ line parameters of the observed masers

Source	α(1950)	δ(1950)	Offset from continuum peak(arc sec)	S [a)] (Jy)	v_{LSR} (km/s)	Δv (km/s)	Photon luminosity [b)] (10^{43} photons s^{-1})	Notes
Orion	- see Matsakis et al.(1980) for details -			50	7.0	1.8	1.4	c)
Orion S-6	——— uncertain ———				∿7.9			d)
W31	$18^h07^m31^s.1$	-19°56'22"	(7, 8)	1.8(0.1)	-8.0	0.8(0.1)	3.0(0.3)	e)
	31.0	56 23	(6, 7)	1.6(0.1)	-6.0	0.6(0.1)	2.2(0.2)	
W33	$18^h11^m15^s.7$	-17°56'53"	(-40, 8)	5.2(0.4)	33.2	0.5(0.1)	4.1(0.4)	
W51	$19^h21^m26^s.2$	14 23'32"	(22,-80)	1.0(0.1)	53.8	0.7(0.2)	2.2(0.2)	f)
	28.8	23 47	(60,-65)	2.9(0.1)	56.8	0.7(0.2)	5.0(0.2)	f)
	27.5	23 52	(40,-60)	0.4(0.1)	59.3	0.7(0.3)	1.2(0.5)	f),g),h)
	25.6	25 41	(13, 49)	1.7(0.1)	64.5	0.7(0.2)	2.3(0.3)	f)
	20.5	24 12	(-66,-40)	0.7(0.1)	66.7	0.8(0.3)	2.6(1.0)	f),i)
DR21	$20^h37^m07^s.6$	42°08'46"	(-73,-21)	13.8(2.4)	-2.6	0.5(0.1)	3.7(0.8)	

Position errors are in the order of ±10" except were noted. Continuum positions are given in table 1.

Notes: a) Fluxes as measured on March 23, 1985 for W31, W51, DR21, as on September 24, 1984 for W33
b) Source distances as given by Wilson et al. (1985) have been used
c) Values for S, v_{LSR} and Δv as given by Matsakis et al. (1980)
d) Spectra taken at the position of Orion S-6 (see Table 1) show evidence for maser activity. However, with the available data it was not possible to determine exact positions and source parameters
e) Position offsets from W31C continuum source (relative offset of the two masers has error of ∿1")
f) Position offsets from W51E continuum source
g) Positions uncertain by ∿30"
h) Source parameters difficult to determine because of blending with thermal emission component
i) Positions uncertain by ∿20"

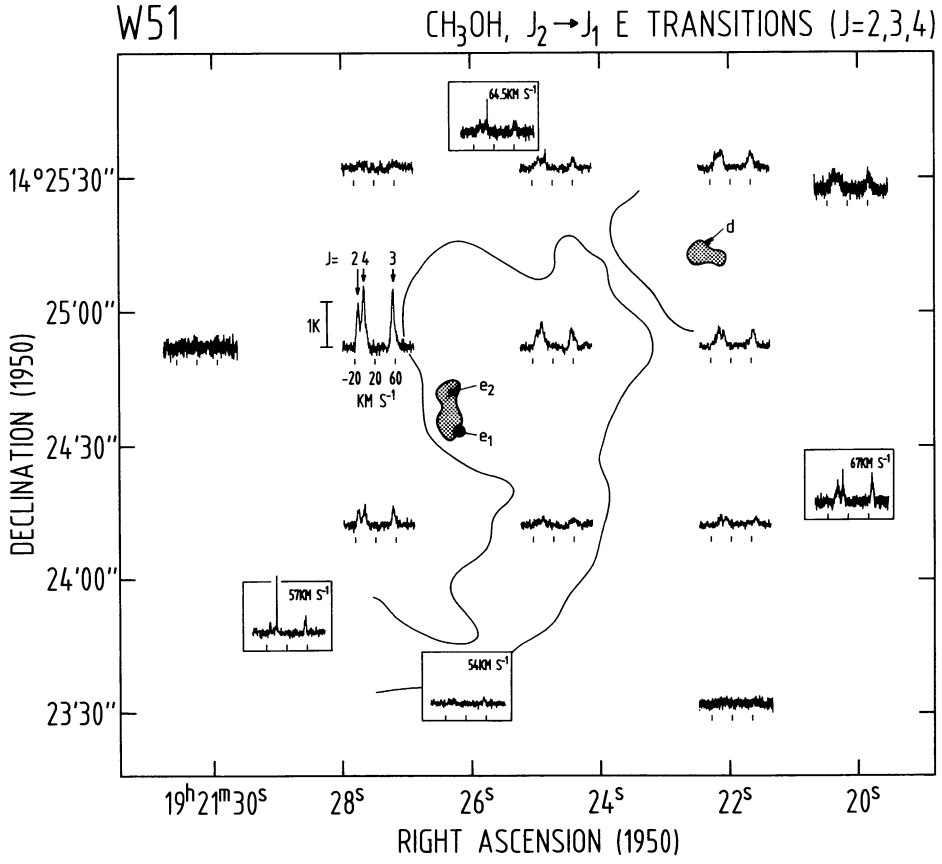

Fig. 4. $J = 2, 3, 4$ spectra towards W51 showing the spatial distribution of the "non-maser" emission features and their relationship to the maser positions. The velocity axis is relative to the rest frequency of the $J = 3$ line. The positions of the $NH_3(3,3)$ hot spots from Ho et al. (1982) are shown shaded and compact H II regions d and e_1,e_2 as given by these authors are indicated as dots. Also shown is the outer contour of the 20 μ map from Genzel et al. (1982). The four boxed spectra are taken close to the maser positions but one should realize that the masers are more apparent in $J = 5, 6$ spectra

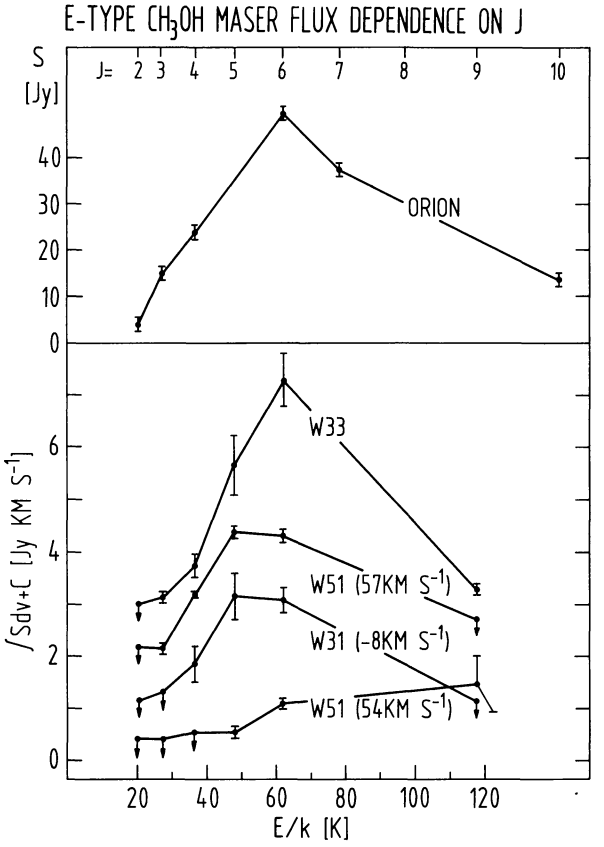

Fig. 5. Integrated flux density for some of the masers observed in this study plotted against the excitation energy of the lower (J_1) state. For comparison, results for the Orion methanol maser from Matsakis et al. (1980) are also shown. For presentation reasons, constants of 0.7, 2.0, and 2.7 Jy km s^{-1} have been added to the W31, W51 (57 km s^{-1}) and W33 data points

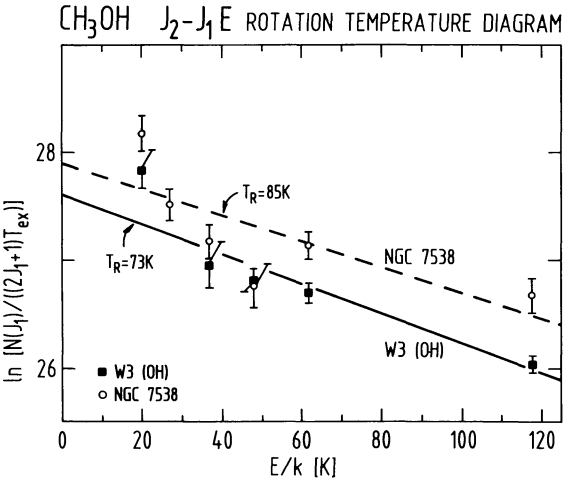

Fig. 6. Normalized column density divided by excitation temperature in level J_1 ($N(J_1)/(g_J T_{ex})$) plotted against the excitation of the J_1 level $E(J_1)$ for the absorption line systems seen towards W3(OH) (squares) and NGC 7538 (circles). The full and dashed lines show fits to a Boltzmann formula for W3(OH) and NGC 7538 respectively

observed the $J = 2 \rightarrow 1$ transitions and found a rapid fall off of intensity with increasing excitation. In fact, the $2_1 \rightarrow 1_1E$ transition was only definitely detected in Orion A and Sgr B2. The "rotation temperature" T_R which one derives from the Gottlieb et al. $2_0 \rightarrow 1_0E$ and $2_{-1} \rightarrow 1_{-1}E$ data is given by:

$$T_L(2_0 \rightarrow 1_0E)/T_L(2_{-1} \rightarrow 1_{-1}E) = 1.33 \exp(-7.5/T_R)$$

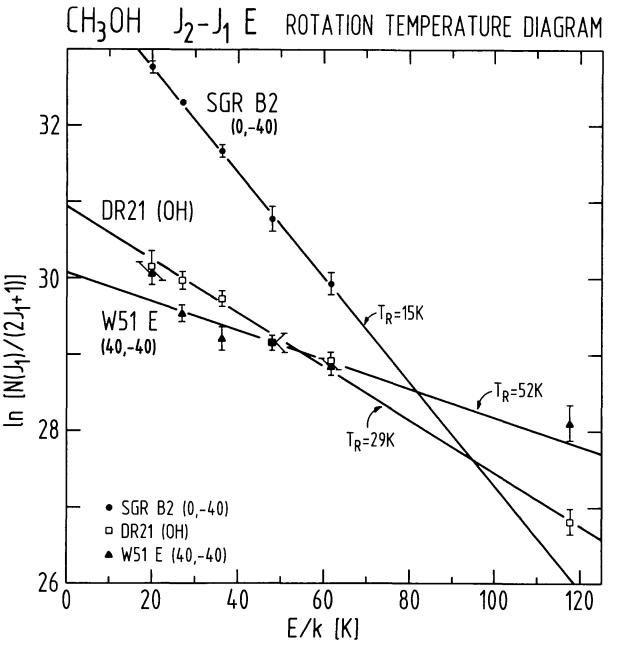

Fig. 7. Normalized column density in level $J_1(N(J_1)/g_J)$ plotted against $E(J_1)$ for the emission lines seen towards selected positions in Sgr B2, DR21 (OH) and W51E

Table 5. CH_3OH rotation temperatures and column densities

Source	Offset[a]	T_R (K)	$N(CH_3OH)$ (10^{15}cm^{-2})	Notes
W3(OH)	(0,0)	130±70	5	b),c)
Sgr B2	(-40,0)	20±1	58	
	(0,-40)	15±1	50	
	(0,0)	21±1	58	
	(0,40)	24±1	60	
	(0,80	19±1	42	
W31C	(0,0)	48±11	7.2	
W33	(0,0)	29±2	9.6	
W51D	(0,0)	60±5	8.4	b),d)
W51E	(0,0)	94±24	18	
	(0,40)	23±4	2.2	
	(40,-40)	52±6	5.6	b)
DR21(OH)	(0,0)	29±2	5.4	b)
DR21	(0,0)	27±3	3.4	

The results were derived from J=2,3,4,5,6 data, except were noted.

Notes:

a) Offsets are relative to the positions given in Table 1

b) J=9 data also available

c) T_R and $N(CH_3OH)$ values for W3(OH) given here were determined using the emission component of the spectra. Values obtained from W3(OH) and NGC7538 absorption data are given in Table 2

d) No J=5 data available

Here we have assumed optically thin emission with $T_{ex} \gg 3$ K. On this basis, we derive $T_R = 8.5$ K for W3(OH), 10.7 K for M17SW, 6.5 K for W51, and 9.2 K for DR21(OH) from Gottlieb et al.'s data. Using these rotation temperatures to predict brightness temperatures in the $J_2 \rightarrow J_1$ series of lines, one finds values of 20 m K or less which is much smaller than our observed intensities. Our derived rotation temperatures (Table 5) are also much greater than the Gottlieb et al. values. We conclude therefore that we are sampling a hotter denser component of the molecular gas than that seen in the 3 mm observations. The cool extended material makes a negligible contribution to our observed intensities. The general agreement of the (broad component) spatial distribution of CH_3OH in W51 and Sgr B2 with the hot ammonia distribution (Mauersberger et al., 1985) causes us to believe that we are observing hot ($T \gtrsim 100$ K) compact (<0.1 pc) regions similar to the compact methanol emission region in Orion. The Orion methanol emission (see Johansson et al., 1984 and references therein) mainly comes from a region smaller than the Onsala 47″ beam and has a rotation temperature of at least 100 K.

A problem which remains is to explain the negative results of Gottlieb et al. in transitions such as $2_1 \rightarrow 1_1 E$ where one would expect on the basis of our results, an observable contribution to the millimeter transition from hot compact methanol regions. Again using the optically thin formulae, one has:

$$T_L(2_1 \rightarrow 1_1)/T_L(2_2 \rightarrow 2_1) = 2.9 \exp(4.6/T_R).$$

The exponential term is likely to be close to unity and hence one expects the intensity of the $2_1 \rightarrow 1_1$ line to be ~ 3 times stronger than $2_2 \rightarrow 2_1$. However, Gottlieb et al. find upper limits to the $2_1 \rightarrow 1_1$ line of order 0.3 K in T_A^* towards W51 and DR21(OH). This compares with our measured main-beam brightness temperatures of order 0.5 K in the $2_2 \rightarrow 2_1$ line. There is thus a discrepancy of roughly a factor 4 which may perhaps be explained by a combination of beam dilution, calibration and pointing errors. Further observations of the 96 GHz lines are needed to settle this question. If the discrepancy should be confirmed, it would suggest that optical depths are high in the $2_1 \rightarrow 1_1$ line.

Another useful test of the validity of the usual optically thin assumptions is to compare our $2_2 \rightarrow 2_1$ data with observations of the $2_1 \rightarrow 3_0 E$ line (Wilson et al., 1985). One has then:

$$\begin{aligned} T_L(2_1 \rightarrow 3_0) &= T_{ex}(2_1 \rightarrow 3_0)\tau(2_1 \rightarrow 3_0) \\ &= 0.45 T_L(2_2 \rightarrow 2_1) = 0.45 T_{ex}(2_2 \rightarrow 2_1)\tau(2_2 \rightarrow 2_1). \end{aligned}$$

We have used here the fact that the 2_1 level is common to both transitions. The available data (e.g. for W51D) suggests that the $2_1 \rightarrow 3_0$ line is weaker than it should be according to the above equation but the result is marginal and we conclude that, for most sources, there is no reason to abandon the usual optically thin assumptions when analysing methanol data (but see discussion of W3(OH) and NGC 7538 above).

The physical parameters in the non-maser methanol regions studied by us are hard to obtain directly. However, one can obtain estimates of these quantities using observations of other molecules which are presumed to be in the methanol region. In the case of W3(OH) for instance (Guilloteau et al., 1983; Mauersberger et al., 1985), the OH and ammonia data suggest a temperature of 80 K and an H_2 density of 10^7 cm^{-3} in a disk of thickness $2\,10^{16}$ cm. As mentioned earlier, the similarity of the line profiles makes it very plausible that ammonia and methanol coexist in this source. In the case of Orion (see Bastien et al., 1985 and references therein), analysis of the formaldehyde data suggests that a region with density 10^6 cm^{-3} and angular extent $\sim 20''$ is responsible for the H_2CO emission. Like methanol (see the limited $2_1 \rightarrow 3_0 E$ map of Wilson et al., 1985), formaldehyde has its peak 20″ south of the KL region. It seems probable therefore that methanol and formaldehyde coexist in this clump and also that similar parameters are applicable to all of the non-maser regions studied by us. Thus, we believe the non-maser methanol emission may come from clumps of dimension 10^{17} cm, temperature 100–200 K, density 10^6–10^7 cm^{-3} and masses of order $1\,M_\odot$. Thus, our methanol observations sample regions much hotter and denser than "normal" molecular cloud gas ($n(H_2) = 10^4$–10^5 cm^{-3}, $T \sim 20$ K).

4.3. *Methanol excitation*

The highest transition observed in this study is the $9_2 \rightarrow 9_1$ which is 82 cm^{-1} or 117 K above the 1_{-1} ground state of *E*-type methanol. The spontaneous decay rate from these levels is $\sim 10^{-3}$ s^{-1} (Lees, 1973). Clearly therefore, if collisions are to account for the observed population of such levels, temperatures upwards of 50 K and densities as high as 10^8 cm^{-3} may be required. In fact, it is likely that in many cases, far infrared radiation (10–50 μ) plays a very important role in accounting for the level populations observed by us. In the Orion compact methanol cloud (Lovas et al., 1982), it is known that torsionally excited methanol transitions are excited and recent observations which we have made show this to be the case also in W3(OH) and NGC 7538. The observed torsionally excited levels are 200 cm^{-1} above ground and have a decay rate of roughly 0.5 s^{-1}. They can be excited by 50 μm radiation, which is present in abundance in most of the sources where we observe non-maser emission or absorption lines. Such radiation will be capable of "pumping" the ground state (see Carroll and Goldsmith, 1981) if:

$$(1 - e^{-\tau_D})/(\exp(h\nu/kT_D) - 1) > A_{rot}/A_{vib} = 2\,10^{-3}. \quad (2)$$

In the above equation τ_D is the dust optical depth at 50 μm in the methanol region, T_D is the dust temperature, $h\nu/k \approx 300$ K is the torsional excitation energy, and (A_{rot}/A_{vib}) is the ratio of rotational to vibrational decay rates. We assume that there is no geometrical dilution or effectively that the dust emission from the methanol cloud itself is responsible for the observed infrared flux. We then have from Eq. (2) that the minimum dust temperature T_D required to account for rotational methanol excitation is 50 K. Such values are not unreasonable and we also may expect optical depths of order unity at 50 microns in the dust associated with the methanol clumps. We conclude therefore that it is highly likely that far infrared excitation of the vibrationally excited levels is responsible for the high populations in the rotationally excited methanol levels observed by us.

A characteristic of far infrared excitation is the selection rule $\Delta k = \pm 1$ but not $= 0$. This has the consequence for infrared excitation followed by subsequent decay that in the vibrational ground state, one has effectively $\Delta k = 0$ or ± 2. One may therefore obtain under certain circumstances a two temperature system of excitation whereby radiation dominates the excitation up *k*-ladders or between even (or odd) *k*'s, while some other process (e.g. collisions) is responsible for the population distribution between odd and even *k*. This sort of situation leads easily to inversion or enhanced absorption in $\Delta k = 1$ transitions of the type discussed in this paper. It is also clear that in cases where

Table 6. Methanol excitation temperatures and optical depths in a two temperature model with column density $10^{17}\,cm^{-2}$ and line width $5\,km\,s^{-1}$. In case A, radiation temperature T_{rad} is 100 K and odd-even temperature T_{0e} is 50 K whereas in case B, T_{rad} is 50 K and T_{0e} is 100 K

Transition	Freq. (GHz)	A		B	
		T_{ex} (K)	τ	T_{ex} (K)	τ
$2_2 - 2_1$	24.93	18.6	3.4	-42.2	-2.1
$6_2 - 6_1$	25.02	18.6	8.3	-42.5	-3.3
$2_1 - 1_1$	96.75	100.	1.9	50.0	5.2
$2_1 - 3_o$	19.97	-22.5	-1.3	13.4	3.0
$2_o - 3_{-1}$	12.2	10.1	4.1	-14.4	-4.3
$4_{-1} - 3_o$	36.2	-49.7	-2.6	20.0	9.0
$5_{-1} - 4_o$	84.5	-347.	-0.9	30.4	13.5

even-to-odd k transitions are inverted, odd-to-even transitions are anti-inverted and vice-versa.

Table 6 shows two sample calculations of methanol excitation temperatures and optical depths for such a two temperature situation. In case A, we have assumed the radiation temperature T_{rad} (that is the temperature up a k-ladder or between odd (even) k levels) to be 100 K and the odd-even temperature T_{0e} to be 50 K. In case B, the reverse is true. In case A, the $J_2 \rightarrow J_1$ sequence is in enhanced absorption whereas in case B, the sequence is inverted. The reverse pattern is shown by transitions such as $2_1 \rightarrow 3_0$ and $4_{-1} \rightarrow 3_0$. One would predict on this basis that the $4_{-1} \rightarrow 3_0$ line should be inverted in W3(OH) but normal in Orion whereas the $2_0 \rightarrow 3_{-1}$ line at 12 GHz should be in absorption in W3(OH) but inverted in Orion. We stress however that the input values to Table 6 are rather arbitrary and quantitative conclusions cannot be drawn from these results. Nevertheless, we find it plausible that (see Wilson et al., 1985) a two temperature situation explains the $2_1 \rightarrow 3_0E$ and $9_2 \rightarrow 10_1A^+$ masers in W3(OH). It is also noteworthy that in sources such as Sgr B2 and W31, the $J_2 \rightarrow J_1$ series is in emission whereas $2_1 \rightarrow 3_0E$ is in absorption (however not $4_{-1} \rightarrow 3_0E$ in Sgr B2, see Morimoto et al., 1984). We conclude therefore that far infrared pumping explains many characteristics of the non-maser-sources which we have studied.

4.4. Methanol abundances

Reliable methanol abundances are hard to obtain on the basis of the present data. This is partly due to optical depth problems but more fundamentally because of the difficulty of deriving the molecular hydrogen column density in the methanol clumps. A crude estimate can be made for the case of W51E where Mauersberger et al. (1985) claim that their ammonia data are consistent with a condensation 10″ (0.4 pc) in size and a density of $2\,10^6\,cm^{-3}$. This estimate depends upon the validity of the virial theorem for the condensation in question and is quite indirect. From Table 5 and taking account of beam dilution, the methanol column density across the clump is of order $2\,10^{17}\,cm^{-2}$ and hence the abundance relative to H_2 is 10^{-7}. This can be compared with the estimate of Irvine and Hjalmarson (1984) for the Orion ridge that $[CH_3OH]/[H_2]$ is $5\,10^{-7}$. We conclude that, given the uncertainties, the difference is not significant and the methanol abundance is normally of order 10^{-7}–10^{-6} in hot condensations.

From our previous discussion, we expect the dust temperature to be high (greater than 50 K) in many of the regions studied by us. At such temperatures, it is likely that lightly bound dust mantles will be evaporated causing changes in relative abundances of molecules in the gas-phase. It would be useful therefore to have methanol abundances for colder regions than those studied by us for comparison. While cold dark clouds do not seem to have been studied in methanol, the results of Gottlieb et al. (1979) suggest that methanol and formaldehyde have comparable abundance in regions with intermediate temperature. Since formaldehyde has a typical dark cloud abundance of order 10^{-8}, there is reason to believe that methanol can be 1–2 orders of magnitude more abundant in hot compact regions than in colder gas.

5. Conclusions

Our main conclusions can be summarised as follows:

1. We have discovered 10 sources of narrow band ($\Delta v \sim 0.3\,km\,s^{-1}$) emission in the $J_2 \rightarrow J_1$ series of E-type methanol emission. By analogy with the known Orion maser sources, we interpret these as being also high-gain masers.

2. The positions of the newly found sources have been determined with an accuracy of approximately 10 arcsec. They in most cases do not agree well with known radio or infrared sources and it is possible that they may be powered by relatively low luminosity objects (10^2–$10^3\,L_\odot$).

3. We have found absorption in the $J_2 \rightarrow J_1$ sequence of lines towards the compact H II regions W3(OH) and NGC 7538. This shows that under certain circumstances, these transitions are not inverted. The apparent rotation temperatures observed are $\sim$80 K suggesting that the lines are formed in a high density high temperature region. From the similarity of the profiles to those known for ammonia, we conclude that methanol coexists with NH_3 in high density clumps surrounding the ionized gas.

4. We have also found emission in the $J_2 \rightarrow J_1$ series with velocities and widths comparable to those found in other transitions. We interpret this as emission from hot clumps embedded in the molecular gas similar to that found south of the Kleinmann-Low region in Orion. These should have densities $\sim 10^6$–$10^7\,cm^{-3}$, temperatures $\sim$100 K, and sizes $\sim$0.1 pc.

5. We conclude that much of our methanol data is compatible with infrared excitation via the 50 μ torsional bands. A consequence of this might be a two temperature excitation situation where either odd-to-even k transitions are inverted and even-to-odd anti-inverted or vice-versa.

6. Very tentatively, we conclude that the abundance ratio $[CH_3OH]/[H_2]$ in hot compact condensations is in the range 10^{-6}–10^{-7} and is higher than in cold extended molecular cloud gas.

Acknowledgements. We would like to take this opportunity to thank O. Lochner and the systems group at Effelsberg for their support of this project. We acknowledge also useful correspondence with R.M. Lees concerning radiative selection rules.

References

Barrett, A.H., Schwartz, P.R., Waters, J.W.: 1971, *Astrophys. J.* **168**, L101

Barrett, A.H., Ho, P., Martin, R.N.: 1975, *Astrophys. J.* **198**, L119

Bastien, P., Batrla, W., Henkel, C., Pauls, T., Walmsley, C.M., Wilson, T.L.: 1985, *Astron. Astrophys.* **146**, 86

Boland, W., de Graauw, Th., Lidholm, S., Lee, T.J.: 1983, *Astrophys. J.* **271**, 183

Buxton, R.B., Barrett, A.H., Ho, P.T.P., Schneps, M.H.: 1977, *Astron. J.* **82**, 985

Carroll, T.J., Goldsmith, P.F.: 1981, *Astrophys. J.* **245**, 891

Genzel, R., Becklin, E.E., Wynn-Williams, C.G., Moran, J.M., Reid, M.J., Jaffe, D.T., Downes, D.: 1982, *Astrophys. J.* **255**, 527

Gottlieb, C.A., Ball, J.A., Gottlieb, E.W., Dickinson, D.F.: 1979, *Astrophys. J.* **227**, 422

Guilloteau, S. Stier, M.T., Downes, D.: 1983, *Astron. Astrophys.* **126**, 10

Henkel, C., Wilson, T.L., Johnston, K.J.: 1984, *Astrophys. J.* **282**, 593

Ho, P.T.P., Genzel, R., Das, A.: 1983, *Astrophys. J.* **266**, 596

Ho, P.T.P., Haschick, A.D.: 1981, *Astrophys. J.* **248**, 622

Irvine, W.M., Hjalmarson, Å.: 1984, Origins of Life **14**, 15

Johannson, L.E.B., Andersson, C., Elldér, J., Friberg, P., Hjalmarson, Å., Höglund, B., Irvine, W.M., Olofsson, H., Rydbeck, G.: 1984, *Astron. Astrophys.* **130**, 227

Johnston, K.J., Henkel, C., Wilson, T.L.: 1984, *Astrophys. J.* **285**, L85

Lees, R.M., Lovas, F.J., Kirchhoff, W.H., Johnson, D.R.: 1973, *J. Phys. Chem. Ref. Data* **2**, 205

Lees, R.M.: 1973, *Astrophys. J.* **184**, 763

Lovas, F.J., Suenram, R.D., Snyder, L.E., Hollis, J.M., Lees, R.M., 1982, *Astrophys. J.* **253**, 149

Matsakis, D.N., Cheung, A.C., Wright, M.C.H., Askne, J.I.H., Townes, C.H., Welch, W.J.: 1980, *Astrophys. J.* **236**, 481

Mauersberger, R., Wilson, T.L., Batrla, W., Walmsley, C.M., Henkel, C.: 1985, *Astron. Astrophys.* **146**, 168

Menten, K.M., Johnston, K.J., Wilson, T.L., Walmsley, C.M., Mauersberger, R., Henkel, C.: 1985, *Astrophys. J. Letters* **293**, L83

Morimoto, M., Ohishi, M., Kanzawa, T.: 1985, *Astrophys. J.* **288**, L11

Pauls, T., Wilson, T.L.: 1980, *Astron. Astrophys.* **91**, L11

Reid, M.J., Moran, J.M.: 1981, *Ann. Rev. Astron. Astrophys.* **19**, 231

Strel'nitskii, V.S.: 1981, *Soviet Astron. Lett.* **7**, 223

Wilson, T.L., Walmsley, C.M., Snyder, L.E., Jewell, P.R.: 1984, *Astron. Astrophys.* **134**, L7

Wilson, T.L., Walmsley, C.M., Menten, K.M., Hermsen, W.: 1985, *Astron. Astrophys.* **147**, L19